Article

Cell Reports

The ID1-CULLIN3 Axis Regulates Intracellular SHH and WNT Signaling in Glioblastoma Stem Cells

Graphical Abstract

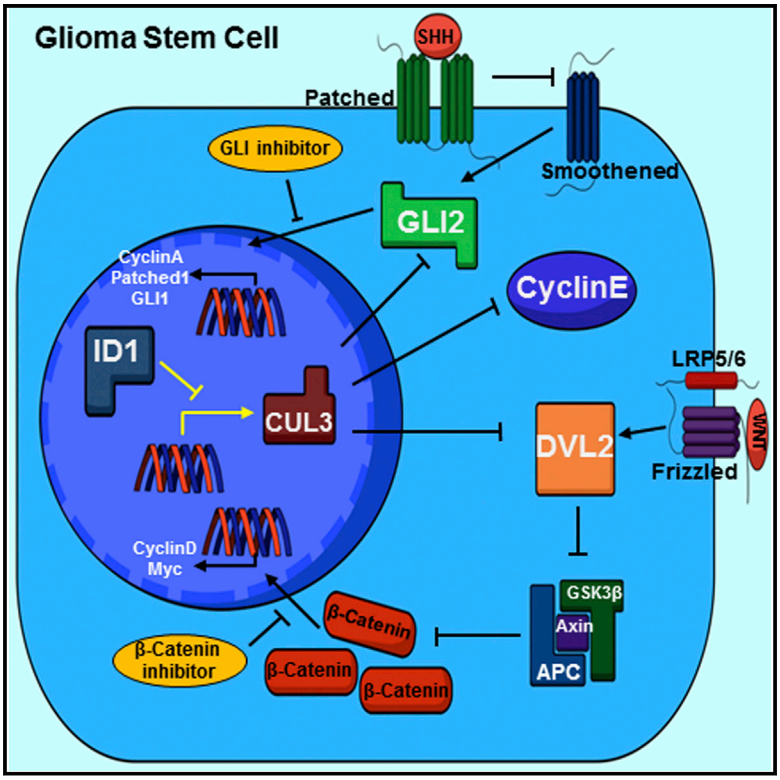

Authors

Xun Jin, Hye-Min Jeon, Xiong Jin, ..., Yunsheng Xu, Jeremy N. Rich, Hyunggee Kim

Correspondence

hg-kim@korea.ac.kr

In Brief

Jin et al. report that the deregulated proteolysis by ID1-mediated suppression of CULLIN3 controls glioblastoma stem cell proliferation, self-renewal, and tumorigenicity by simultaneously activating intracellular WNT and SHH signaling. The findings provide a rationale for therapeutic intervention targeting multiple intracellular cancer stemness signaling pathways.

Highlights

- ID1 suppresses CULLIN3, which activates GSC self-renewal via SHH and WNT signaling
- CULLIN3 regulates ubiquitin-mediated degradation of DVL2 and GLI2 proteins
- The combined controls of GLI2 and β-CATENIN effectively suppress GSC properties
- The ID1^{hi}/CULLIN3^{lo} signature correlates with poor prognosis of GBM patients

Accession Numbers

GSE40614

Jin et al., 2016, Cell Reports *16*, 1629–1641
August 9, 2016
http://dx.doi.org/10.1016/j.celrep.2016.06.092

Cell Reports
Article

The ID1-CULLIN3 Axis Regulates Intracellular SHH and WNT Signaling in Glioblastoma Stem Cells

Xun Jin,[1,2,5,6,7] Hye-Min Jeon,[1,7] Xiong Jin,[1] Eun-Jung Kim,[1] Jinlong Yin,[3] Hee-Young Jeon,[1] Young-Woo Sohn,[1] Se-Yeong Oh,[1] Jun-Kyum Kim,[1] Sung-Hak Kim,[1,4] Ji-Eun Jung,[1,3] Sungwook Kwak,[1] Kai-Fu Tang,[5] Yunsheng Xu,[5] Jeremy N. Rich,[2] and Hyunggee Kim[1,*]

[1]Department of Biotechnology, College of Life Sciences and Biotechnology, Korea University, Seoul 02841, Republic of Korea
[2]Department of Stem Cell Biology and Regenerative Medicine, Lerner Research Institute, Cleveland Clinic, Cleveland, OH 44195, USA
[3]Specific Organs Cancer Division, Research Institute and Hospital, National Cancer Center, Goyang 10408, Republic of Korea
[4]Department of Neurosurgery, University of Alabama at Birmingham, Birmingham, AL 35294, USA
[5]First Affiliated Hospital of Wenzhou Medical University, Wenzhou 325015, Zhejiang, P.R. China
[6]Tianjin Medical University Cancer Institute and Hospital, Tianjin 300060, P.R. China
[7]Co-first author
*Correspondence: hg-kim@korea.ac.kr
http://dx.doi.org/10.1016/j.celrep.2016.06.092

SUMMARY

Inhibitor of differentiation 1 (ID1) is highly expressed in glioblastoma stem cells (GSCs). However, the regulatory mechanism responsible for its role in GSCs is poorly understood. Here, we report that ID1 activates GSC proliferation, self-renewal, and tumorigenicity by suppressing CULLIN3 ubiquitin ligase. ID1 induces cell proliferation through increase of CYCLIN E, a target molecule of CULLIN3. ID1 overexpression or CULLIN3 knockdown confers GSC features and tumorigenicity to murine *Ink4a/Arf*-deficient astrocytes. Proteomics analysis revealed that CULLIN3 interacts with GLI2 and DVL2 and induces their degradation via ubiquitination. Consistent with ID1 knockdown or CULLIN3 overexpression in human GSCs, pharmacologically combined control of GLI2 and β-CATENIN effectively diminishes GSC properties. A ID1-high/CULLIN3-low expression signature correlates with a poor patient prognosis, supporting the clinical relevance of this signaling axis. Taken together, a loss of CULLIN3 represents a common signaling node for controlling the activity of intracellular WNT and SHH signaling pathways mediated by ID1.

INTRODUCTION

Glioblastoma (GBM), the most prevalent and malignant primary brain tumor, has been extensively characterized at the molecular level, but these findings have not been translated into effective molecularly targeted therapies (Wen and Kesari, 2008). This failure may be due to the presence of self-renewing, highly tumorigenic, stem-like cancer cells commonly referred to as GBM stem cells (GSCs; Singh et al., 2004). Although the exact identity of GSCs remains controversial in terms of enrichment markers and cell of origin, these cells display therapeutic resistance, invasion into normal brain, angiogenesis, and immune escape (Lathia et al., 2015; Tanaka et al., 2013; Yi et al., 2011). Like neural stem cells (NSCs), GSCs are functionally defined through assays of stem cell marker expression, self-renewal, sustained proliferation, and differentiation potential. However, GSCs are distinguished from NSCs by their chromosomal alterations, cytologic and nuclear atypia, aberrant differentiation, failure to respond growth inhibitory cues, and tumor growth. Thus, GSCs may be differentially regulated from NSCs via alternative molecular targets. Several studies have shown that GSCs have selective dependence on molecular targets, including AKT (Bleau et al., 2009), inducible nitric oxide synthase (Eyler et al., 2011), bone marrow X-linked kinase (Guryanova et al., 2011), pigment epithelium-derived factor (Yin et al., 2015), GREMLIN1 (Yan et al., 2014), and LIM-domain only 2 (Kim et al., 2015).

The inhibitor of differentiation (ID) family of proteins critically regulates normal neural development and gliomagenesis. ID1 leads to anchorage-independent growth of both NSCs and GSCs through RAP1GAP signaling (Niola et al., 2012, 2013). We previously suggested that ID3 controls epidermal growth factor receptor (EGFR) signaling-mediated GSC genesis and perivascular niche formation through regulation of the angiogenic cytokines GRO1, interleukin-6 (IL-6), and IL-8 (Jin et al., 2011), indicating that IDs autonomously support the GSC niche. Additionally, transforming growth factor β (TGF-β) was shown to increase GSC self-renewal through SMAD regulation of ID1 and ID3, which, in turn, control the expression of stem cell factors, such as LIF, SOX2, and SOX4 (Anido et al., 2010). Platelet-derived growth factor (PDGF) increased ID4 expression by activating nitric oxide signaling, and subsequently ID4 induces expression of JAGGED1, one of NOTCH receptor ligands, by suppressing miR129 (Jeon et al., 2014). PDGF-ID4-NOTCH signaling node is activated in GSCs and tumor endothelial cells in the perivascular microenvironment and accelerates glioma progression.

Stem cell signaling pathways, such as NOTCH, WNT, and SHH, are frequently deregulated in a variety of human

malignancies and directly induce tumor development and progression. Thus, targeting these deregulated stem cell signaling pathways is considered promising therapeutic intervention to eliminate caner stem cells (Takebe et al., 2011).

NOTCH receptors are expressed in both low-grade and high-grade gliomas and serve not only as glioma grading and plausible prognostic factors, but also as therapeutic targets (Dell'albani et al., 2014). Furthermore, several studies have demonstrated that NOTCH signaling modulates GSC traits that are selectively expressed by various transcriptional regulators, including ID3 (Jin et al., 2011), ID4 (Jeon et al., 2008), interferon regulatory factor 7 (Jin et al., 2012), and hypoxia inducible factor 1α (Qiang et al., 2012).

In contrast to the widely reported NOTCH signaling activation in GBM mainly by the classical JAGGED and NOTCH interaction, the WNT and SHH signaling in GBM is not mediated by their ligands' and receptors' interaction. Instead, WNT and SHH signaling pathways in these tumors are activated by deregulation of these signaling pathways related components in respective signaling pathways: ASCL1 (Rheinbay et al., 2013) and PKM2 (Yang et al., 2011) for WNT/β-CATENIN signaling, and PTCH1 (Munoz et al., 2015) and GLI (Becher et al., 2008) for SHH signaling. These findings indicate that WNT and SHH signaling mechanisms in GBM are distinct from those induced in other human malignancies, and improved understanding of these signaling pathways is urgently needed to provide better control of GBM.

We now report that ID1 controls GSCs through suppression of Cullin3 E3 ubiquitin ligase. CULLIN3 suppression simultaneously activates ligand-independent WNT and SHH signaling by increasing DVL2 and GLI2 protein levels, respectively. Thus, CULLIN3 represents a common signaling node controlling the activity of multiple essential GSC signaling pathways mediated by ID1.

RESULTS

Ectopic ID1 Expression Confers Tumorigenic Ability to Primary Mouse *Ink4a/Arf*$^{-/-}$ Astrocyte Cells

To assess tumorigenic potential of ID1, we overexpressed ID1 in non-transformed murine astrocytes with targeted disruption of $p16^{Ink4a}$ and $p19^{Arf}$ (*Ink4a/Arf*$^{-/-}$ astrocytes), two frequently inactivated tumor suppressors in human glioblastoma (Cancer Genome Atlas Research Network, 2008). ID1 overexpression significantly accelerated cell growth (Figure S1A), including a "piled up" morphology (a typical property of cancer cells) after confluence (Figure S1B). Furthermore, soft agar analysis revealed the anchorage-independent growth of *Ink4a/Arf*$^{-/-}$ astrocytes expressing ID1 (*Ink4a/Arf*$^{-/-}$ astrocyte-ID1 cells; Figure S1C).

ID1 Suppresses the CULLIN3 E3 Ubiquitin Ligase and Increases CYCLIN E Protein Stability

Because increased cell proliferation is one of the obvious phenotypic changes in *Ink4a/Arf*$^{-/-}$ astrocyte-ID1 cells, we examined expression levels of CYCLINs in these cells. Immunoblot analysis showed that CYCLIN E, CYCLIN D, and CYCLIN A proteins increased in *Ink4a/Arf*$^{-/-}$ astrocyte-ID1 cells compared to control *Ink4a/Arf*$^{-/-}$ astrocytes (Figure 1A). The change in CYCLIN D and CYCLIN A proteins by ID1 overexpression was correlated with an increase in mRNA levels. However, *Cyclin E* mRNA levels did not increase in response to ID1 overexpression (Figure 1B). In lieu of this, we examined the protein half-life of CYCLIN E in *Ink4a/Arf*$^{-/-}$ astrocyte-ID1 cells using a translation inhibitor (cycloheximide [CHX]) and found that ID1 overexpression markedly increased CYCLIN E protein stability (Figures 1C and S1D).

Because CYCLIN E protein stability is primarily regulated by ubiquitination (Singer et al., 1999), we examined expression levels of several ubiquitin ligases in *Ink4a/Arf*$^{-/-}$ astrocyte-ID1 cells and found that CULLIN3 was markedly decreased following ID1 overexpression (Figure 1D), indicating that CULLIN3 may be a key downstream target of ID1. We found that there are six E-box elements (binding sites of bHLH transcription factors) located in the *Cullin3* promoter (up to −1267 bp upstream of the transcriptional start site). A luciferase reporter assay using a *Cullin3*-promoter construct revealed that ID1 significantly repressed *Cullin3* promoter activity in a dose-dependent manner (Figure 1E), indicating that ID1 mediates transcriptional suppression of *Cullin3*. Moreover, CYCLIN E expression increased following CULLIN3 knockdown in *Ink4a/Arf*$^{-/-}$ astrocytes (Figure 1F) and decreased upon CULLIN3 overexpression in *Ink4a/Arf*$^{-/-}$ astrocyte-ID1 cells (Figure 1G). Fluorescence-activated cell sorting (FACS) analysis revealed that ID1 overexpression and CULLIN3 knockdown in the *Ink4a/Arf*$^{-/-}$ astrocytes increased the S phase cell population with markedly reduction in the G_0/G_1 and G_2/M phase populations. However, CULLIN3 overexpression in *Ink4a/Arf*$^{-/-}$ astrocyte-ID1 cells led to dramatic increase in G_0/G_1 and G_2/M phase populations (Figure 1H). Taken together, these results indicate that the ID1-CULLIN3 regulatory axis plays a crucial role in the *Ink4a/Arf*$^{-/-}$ astrocyte proliferation.

ID1-Mediated Suppression of CULLIN3 Confers GSC Features and a Malignant Glioblastoma-Forming Ability to *Ink4a/Arf*$^{-/-}$ Astrocytes

Of interest, ID1 overexpression in *Ink4a/Arf*$^{-/-}$ astrocytes also led to reduced expression of the differentiated astrocyte marker, GFAP, and increased expression of the neural stem cell marker, NESTIN (Figure S1E). Thus, we speculated that ID1-mediated suppression of CULLIN3 may render *Ink4a/Arf*$^{-/-}$ astrocytes less differentiated. To elucidate role of ID1 in GSCs genesis, we examined sphere forming ability (a surrogate marker of GSCs self-renewal), stem cell marker expression, and tumorigenicity.

We found that ID1 overexpression or CULLIN3 knockdown in *Ink4a/Arf*$^{-/-}$ astrocytes increased sphere formation, whereas restoration of CULLIN3 in *Ink4a/Arf*$^{-/-}$ astrocyte-ID1 cells significantly decreased sphere formation (Figures 2A, 2B, S2A, and S2B). However, CYCLIN E overexpression alone did not impart sphere-forming ability to *Ink4a/Arf*$^{-/-}$ astrocytes, and that CYCLIN E knockdown failed to inhibit the sphere formation of *Ink4a/Arf*$^{-/-}$ astrocyte-ID1 cells (Figures 2A, 2B, and S2C). FACS analysis revealed that stem cell markers NESTIN- and SOX2-positive cells were markedly enriched in *Ink4a/Arf*$^{-/-}$ astrocyte-ID1 and *Ink4a/Arf*$^{-/-}$ astrocyte-shCULLIN3

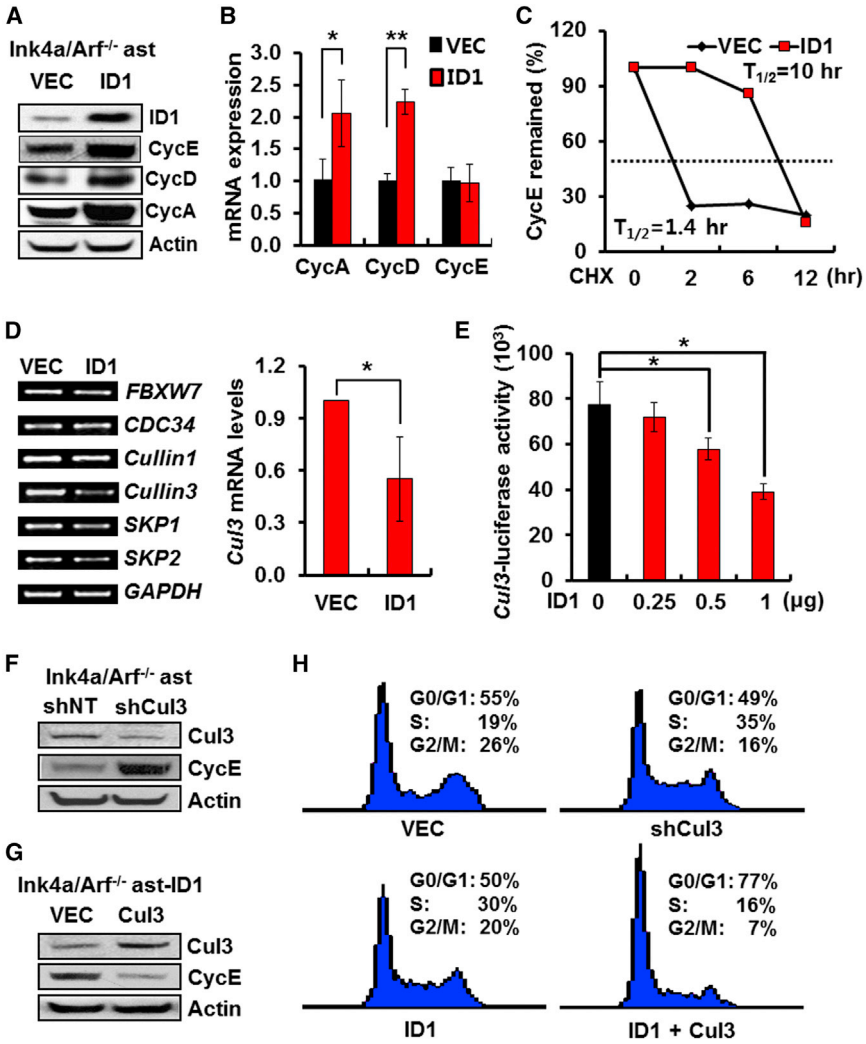

Figure 1. ID1 Transcriptionally Represses Expression of the E3 Ubiquitin Ligase, *Cullin3*

(A) CYCLIN A, D, and E protein levels in *Ink4a/Arf*$^{-/-}$ astrocyte-ID1 and control *Ink4a/Arf*$^{-/-}$ astrocytes (VEC).

(B) *Cyclin A*, *D*, and *E* mRNA levels in *Ink4a/Arf*$^{-/-}$ astrocyte-ID1 and control *Ink4a/Arf*$^{-/-}$ astrocytes (VEC). *p < 0.05; **p < 0.01 (n = 3). Data are mean ± SD.

(C) CYCLIN E protein degradation in *Ink4a/Arf*$^{-/-}$ astrocyte-ID1 and control *Ink4a/Arf*$^{-/-}$ astrocytes (VEC) following exposure to cycloheximide (CHX, 50 μM) for the indicated times.

(D) The mRNA expression levels of several E3 ubiquitin ligases in *Ink4a/Arf*$^{-/-}$ astrocyte-ID1 and control *Ink4a/Arf*$^{-/-}$ astrocytes (VEC). A right graph shows quantitative level of *Cullin3* mRNA in these cells. *p < 0.05 (n = 3). Data are mean ± SD.

(E) *Cullin3*-promoter luciferase reporter activity in the presence (0.25–1 μg) or absence of ID1. *p < 0.05 (n = 3). Data are mean ± SD.

(F) CULLIN3 and CYCLIN E protein levels in *Ink4a/Arf*$^{-/-}$ astrocytes and *Ink4a/Arf*$^{-/-}$ astrocyte-shCULLIN3 cells.

(G) CULLIN3 and CYCLIN E protein levels in *Ink4a/Arf*$^{-/-}$ astrocyte-ID1 and *Ink4a/Arf*$^{-/-}$ astrocyte-ID1-CULLIN3 cells.

(H) Cell cycle of *Ink4a/Arf*$^{-/-}$ astrocytes, *Ink4a/Arf*$^{-/-}$ astrocyte-ID1, *Ink4a/Arf*$^{-/-}$ astrocyte-shCULLIN3, and Ink4a/Arf$^{-/-}$ astrocyte-ID1-CULLIN3 cells was analyzed by FACS.

cells, but not in *Ink4a/Arf*$^{-/-}$ astrocyte-VEC and *Ink4a/Arf*$^{-/-}$ astrocyte-CYCLIN E cells (Figure 2C). Conversely, differentiated astrocyte cell marker S100β-positive cells, which are a major subpopulation in *Ink4a/Arf*$^{-/-}$ astrocyte-VEC and *Ink4a/Arf*$^{-/-}$ astrocyte-CYCLIN E cells, dramatically decreased in *Ink4a/Arf*$^{-/-}$ astrocyte-ID1 and *Ink4a/Arf*$^{-/-}$ astrocyte-shCULLIN3 cells (Figure 2C). Next, we compared the brain tumor-initiating ability of *Ink4a/Arf*$^{-/-}$ astrocyte-ID1, *Ink4a/Arf*$^{-/-}$ astrocyte-CYCLIN E, *Ink4a/Arf*$^{-/-}$ astrocyte-shCULLIN3, and *Ink4a/Arf*$^{-/-}$ astrocyte-VEC cells using orthotopic injection model. *Ink4a/Arf*$^{-/-}$ astrocyte-ID1 and *Ink4a/Arf*$^{-/-}$ astrocyte-shCULLIN3 cells, but not *Ink4a/Arf*$^{-/-}$ astrocyte-CYCLIN E and *Ink4a/Arf*$^{-/-}$ astrocyte-VEC cells, gave rise to brain tumors (Figure 2D) displaying histological features associated with high-grade glioma, such as focal necrosis, high invasiveness, massive hemorrhage, and pleomorphic nuclei of tumor cells (Figure 2E). Taken together, these in vitro and in vivo results suggest that ID1-mediated suppression of CULLIN3 confers stem cell-like features and tumorigenicity to *Ink4a/Arf*$^{-/-}$ astrocytes.

ID1-CULLIN3 Axis Controls CYCLIN E, DVL2, and GLI2 Protein Polyubiquitination

Because CULLIN3 is an E3 ubiquitin ligase, interaction of CULLIN3 with proteins is an important event to regulate protein degradation. To understand the molecular mechanisms underlying the acquisition of GSCs feature and tumorigenicity in *Ink4a/Arf*$^{-/-}$ astrocytes by the ID1-CULLIN3 regulatory axis, we employed immunoprecipitation of Flag-CULLIN3 in HEK293T cells followed by MALDI-TOF mass spectroscopy (MALDI-TOF MS) to identify CULLIN3-interacting proteins. The method was validated by identifying four CYCLIN E peptides that interact with CULLIN3 (Figure 3A). Of interest, we identified GLI2 and DVL2 as CULLIN3-interacting proteins, which are involved in the SHH and WNT signaling pathways, respectively (Figures 3A and 3B), and therefore would link the ID1-CULLIN3 axis with stem cell signaling. The interactions of CULLIN3 with CYCLIN E, GLI2, and DVL2 were further confirmed by immunoprecipitation of Flag-CYCLIN E and Myc-CULLIN3 (Figure 3C), Myc-GLI2 and Flag-CULLIN3 (Figure 3D), and Flag-DVL2 and Myc-CULLIN3 (Figure 3E), respectively. Poly-ubiquitinated CYCLIN E, GLI2, and DVL2 levels were reduced by ID1 overexpression but were recovered by co-expression of CULLIN3 with ID1 (Figures 3F–3H). The luciferase reporter assays revealed that SHH (Gli-BS-luciferase) and WNT/β-catenin signaling

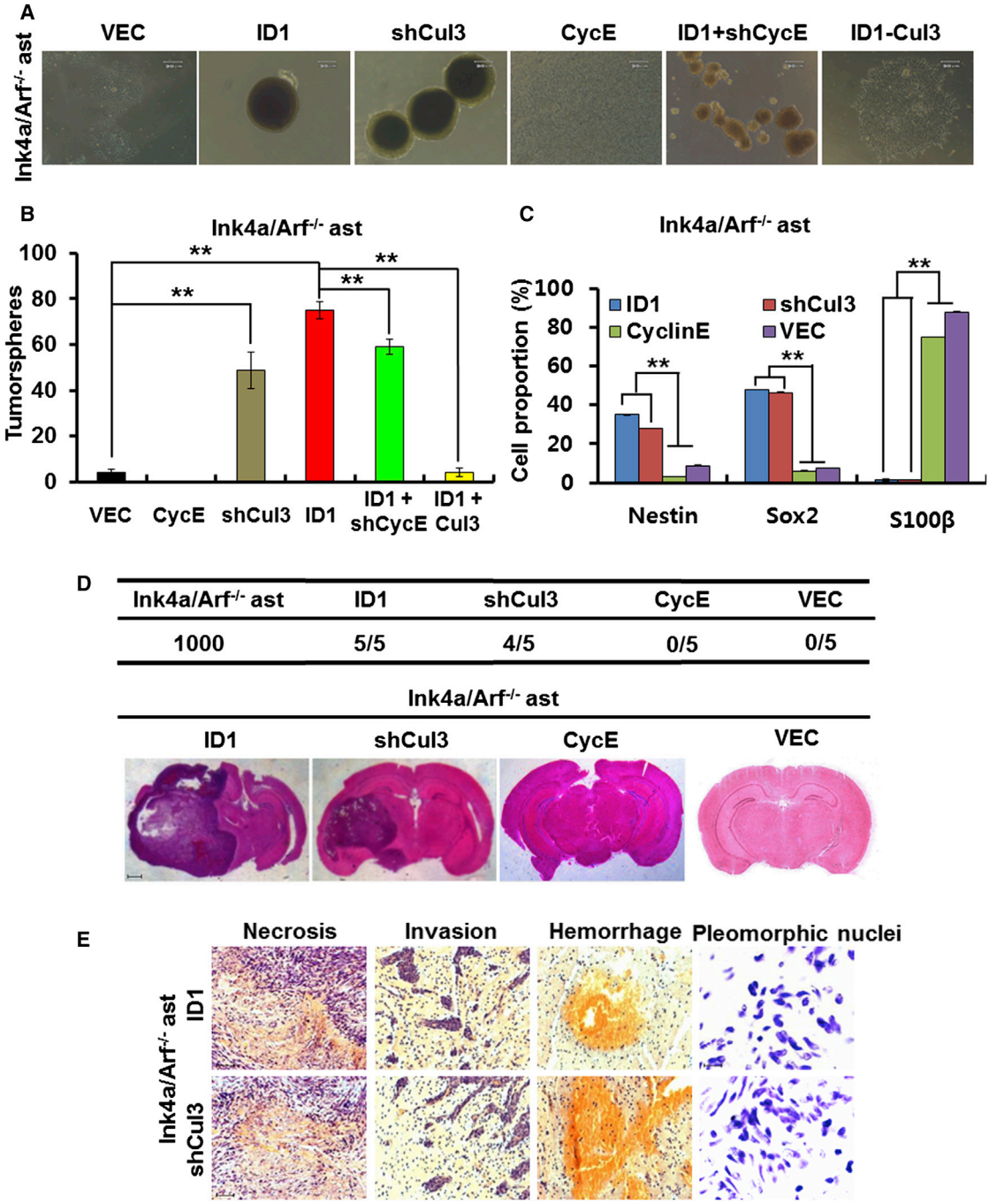

Figure 2. The ID1-CULLIN3 Regulatory Axis Stimulates GSC Genesis and Malignant Glioma Formation

(A) Representative photos showing tumorspheres generated from *Ink4a/Arf*$^{-/-}$ astrocytes expressing empty vector (VEC; shNT+Puro), ID1, shCULLIN3, CYCLIN E, ID1+shCYCLIN E, and ID1+CULLIN3. Scale bar, 20 μm.

(B) Tumorsphere formation ability of *Ink4a/Arf*$^{-/-}$ astrocytes expressing empty vector (VEC), CYCLIN E, shCULLIN3, ID1, ID1+shCYCLIN E, and ID1+CULLIN3. **$p < 0.01$ ($n = 3$). Data are mean ± SD.

(C) FACS shows NESTIN^{+}, SOX2^{+}, and S100β^{+} cell proportions in the *Ink4a/Arf*$^{-/-}$ astrocyte-VEC, *Ink4a/Arf*$^{-/-}$ astrocyte-ID1, *Ink4a/Arf*$^{-/-}$ astrocyte-shCULLIN3, and *Ink4a/Arf*$^{-/-}$ astrocyte-CYCLIN E. **$p < 0.01$ ($n = 3$). Data are mean ± SD.

(D) The tumor-forming frequency of *Ink4a/Arf*$^{-/-}$ astrocyte-VEC, *Ink4a/Arf*$^{-/-}$ astrocyte-ID1, *Ink4a/Arf*$^{-/-}$ astrocyte-shCULLIN3, and *Ink4a/Arf*$^{-/-}$ astrocyte-CYCLIN E post-orthotopic implantation (upper table). Representative H&E staining of mice whole brains implanted with *Ink4a/Arf*$^{-/-}$ astrocyte-shCULLIN3, and *Ink4a/Arf*$^{-/-}$ astrocyte-CYCLIN E (lower images). Scale bar, 2 mm.

(E) Representative images of H&E staining showing histopathological features of brain tumors. Scale bar, 250 μm.

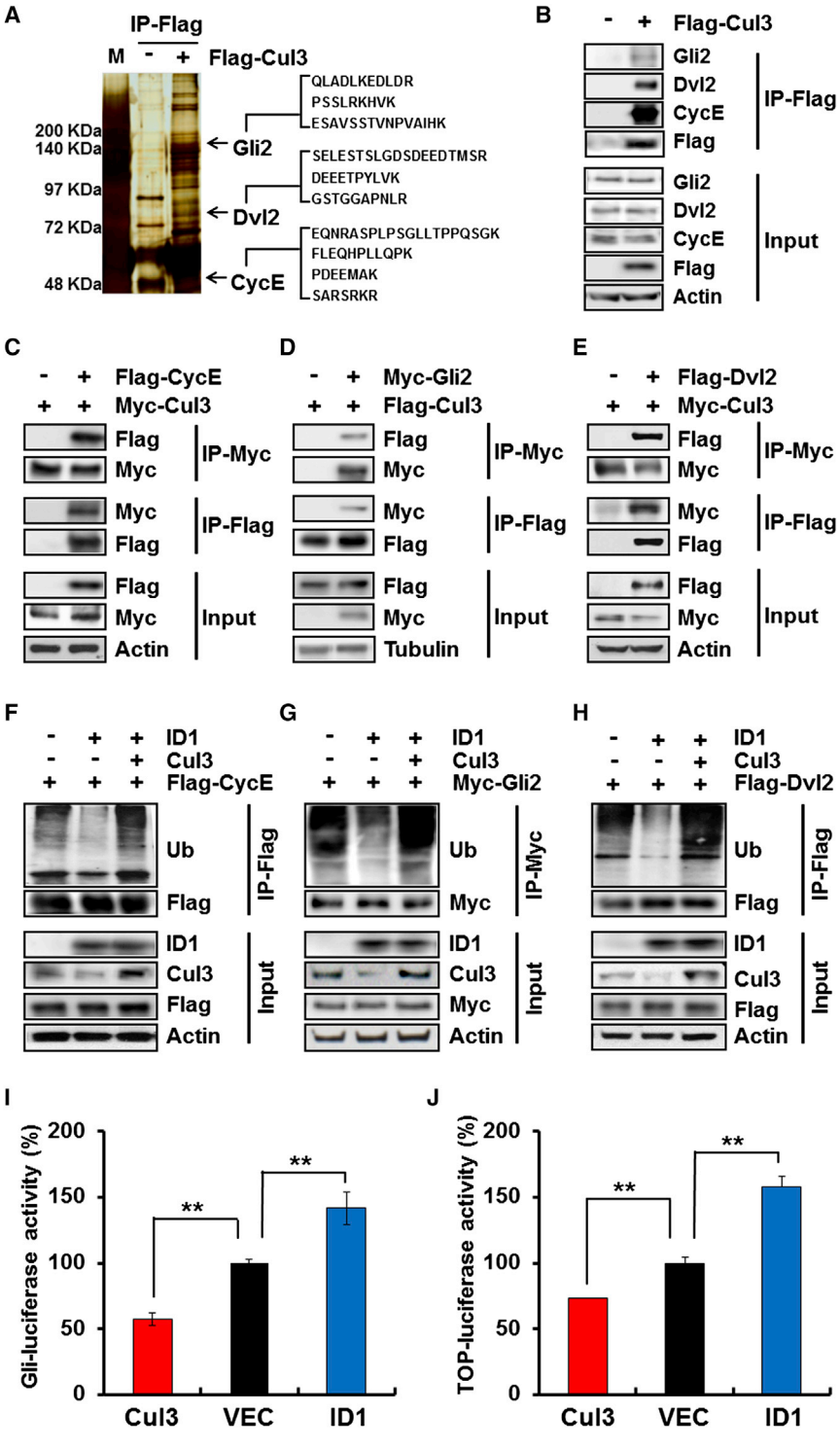

Figure 3. ID1 Inhibits CYCLIN E, GLI2, and DVL2 Protein Degradation through CULLIN3 Repression

(A) Immunoprecipitation was performed using anti-Flag M2 affinity resin and extracts of HEK293T cells transfected with Flag-CULLIN3. The immunoprecipitated protein complex was visualized by silver staining and identified by MALDI-TOF MS analysis. The identified peptide sequences of GLI2, DVL2, and CYCLIN E are shown in the right panel.

(B) Interactions of CULLIN3 with GLI2, DVL2, and CYCLIN E were confirmed using immunoprecipitation-western blot analyses in HEK293T cells.

(C–E) Interactions of CULLIN3 with CYCLIN E (C), GLI2 (D), and DVL2 (E) were confirmed by ectopic expression of Myc- or Flag-tagging exogenous genes in HEK293T cells.

(F–H) Polyubiquitination of CYCLIN E (F), GLI2 (G), and DVL2 (H) by the ID1-CULLIN3 regulatory axis in HEK293T cells.

(I) HEK293T cells were co-transfected with pGL3-Gli-BS (containing Gli-binding sites) and ID1 or CULLIN3, plus the corresponding control vector. $^{**}p < 0.01$ (n = 3). Data are mean ± SD.

(J) HEK293T cells were co-transfected with pTOP-FLASH (containing TCF/LEF-binding sites) and ID1 or CULLIN3, plus the corresponding control vector. $^{**}p < 0.01$ (n = 3). Data are mean ± SD.

(pTOP-luciferase) activities were increased by ID1 overexpression and were markedly reduced by CULLIN3 overexpression (Figures 3I and 3J). Taken together, these results indicate that ID1-mediated suppression of CULLIN3 may activate SHH and WNT signaling by stabilizing GLI2 and DVL2 proteins, respectively.

ID1-CULLIN3 Regulatory Axis Activates Intracellular WNT and SHH Signaling in *Ink4a/Arf*$^{-/-}$ Astrocytes

To confirm the functional significance of the biochemical findings from our glioblastoma models, we performed immunoprecipitations with CULLIN3-specific antibodies in *Ink4a/Arf*$^{-/-}$ astrocyte-ID1 and *Ink4a/Arf*$^{-/-}$ astrocyte-VEC cells. ID1 overexpression markedly reduced the interactions of CULLIN3 with either DVL2 or GLI2 through suppression of CULLIN3 expression (Figure 4A). To identify poly-ubiquitinated GLI2 and DVL2 levels, we performed immunoprecipitations and denature immunoprecipitations with GLI2- and DVL2-specific antibodies. Poly-ubiquitinated GLI2 and DVL2 levels were reduced by CULLIN3 knockdown in *Ink4a/Arf*$^{-/-}$ astrocytes (Figures 4B and S2D). Furthermore, we examined the protein half-life of DVL2 and GLI2 in *Ink4a/Arf*$^{-/-}$ astrocyte-VEC, *Ink4a/Arf*$^{-/-}$ astrocyte-ID1, and *Ink4a/Arf*$^{-/-}$ astrocyte-ID1+CULLIN3 cells by CHX treatment. ID1 overexpression markedly increased DVL2 and GLI2 protein stability relative to VEC and ID1+CULLIN3-overexpressing cells (Figures S2E and S2F). However, qRT-PCR analysis revealed that *Dvl2* and *Gli2* mRNA levels were not significantly changed by ID1 overexpression

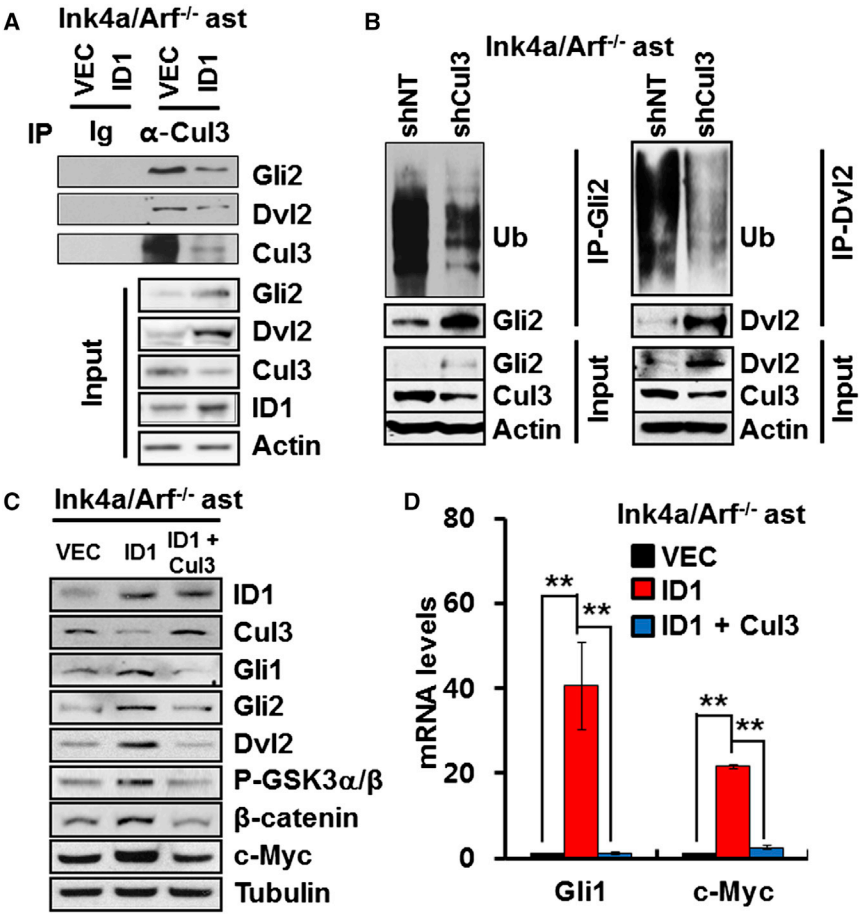

Figure 4. ID1-CULLIN3 Axis Activates WNT and SHH Pathways in *Ink4a/Arf*$^{-/-}$ Astrocytes

(A) Interactions of endogenous CULLIN3 with GLI2 or DVL2 in *Ink4a/Arf*$^{-/-}$ astrocyte-ID1 and control *Ink4a/Arf*$^{-/-}$ astrocytes.

(B) Polyubiquitination of GLI2 and DVL2 in *Ink4a/Arf*$^{-/-}$ astrocyte-shCULLIN3 and control *Ink4a/Arf*$^{-/-}$ astrocytes.

(C) SHH (GLI1 and GLI2) and WNT (P-GSK3α/β, β-CATENIN and c-MYC) signaling protein levels in *Ink4a/Arf*$^{-/-}$ astrocytes, *Ink4a/Arf*$^{-/-}$ astrocyte-ID1, and *Ink4a/Arf*$^{-/-}$ astrocyte-ID1-CULLIN3.

(D) Expression levels of *Gli1* and *c-Myc* mRNAs in *Ink4a/Arf*$^{-/-}$ astrocytes, *Ink4a/Arf*$^{-/-}$ astrocyte-ID1, and *Ink4a/Arf*$^{-/-}$ astrocyte-ID1-CULLIN3. $^{**}p < 0.01$ (n = 3). Data are mean ± SD.

(Figure S2G). These results indicate that ID1 regulates DVL2 and GLI2 expression at a post-transcriptional level by suppressing CULLIN3 expression. Simultaneous activation of SHH and WNT signaling by the ID1-CULLIN3 regulatory axis was confirmed by the protein levels of GLI2, GLI1 (increased by SHH signaling; Ruiz i Altaba, 1998), DVL2, p-GSK3α/β, β-CATENIN, and c-MYC (a target gene of WNT/β-CATENIN signaling) in *Ink4a/Arf*$^{-/-}$ astrocyte-VEC, *Ink4a/Arf*$^{-/-}$ astrocyte-ID1, and *Ink4a/Arf*$^{-/-}$ astrocyte-ID1+CULLIN3 cells (Figure 4C). The increased *Gli1* and *c-Myc* mRNA levels observed in *Ink4a/Arf*$^{-/-}$ astrocyte-ID1 cells were dramatically reduced by CULLIN3 restoration (*Ink4a/Arf*$^{-/-}$ astrocyte-ID1+CULLIN3 cells; Figure 4D). These results suggest the ID1-CULLIN3 axis acts as a ligand-independent upstream regulator of SHH/WNT signaling.

ID1 Regulates Cancer Stem Cell Properties and SHH/WNT Signaling in Primary Human GSCs

To elucidate the biological effects of ID1-CULLIN3 axis in GSCs, we first found that ID1 expression was significantly increased in various GSCs derived from patients with glioblastoma (Figure S3A), and CULLIN3 expression was significantly decreased in several GSCs (Figure S3B). An inverse correlation was observed between ID1 and CULLIN3 expression in GSCs (Figure S3C). Then, we generated two ID1 knockdown (KD) GSC cultures; GSC8 (expressing high levels of ID1) and GSC2 (expressing moderate levels of ID1) using two non-overlapping ID1-3′ UTR targeting short hairpin RNAs (shRNAs), and along with a non-targeting shRNA sequence (shNT) to rule out off-target effects. In vitro limiting dilution assay revealed that ID1 depletion using ID1 3′-UTR-targeted shRNAs significantly reduced tumorsphere-forming ability of GSC8 cells, and that re-overexpression of ID1-coding DNA sequence (CDS) rescued tumorsphere-forming ability in ID1-depleted GSCs (Figures 5A and S3D). A previous study has demonstrated that ID1 and ID3 have a possible overlapping function in mouse embryo development (Lyden et al., 1999). Therefore, we examined the role of ID3 in tumorsphere-forming ability of ID1-depleted GSCs. Ectopic ID3 expression did not significantly rescue tumorsphere-forming ability in ID1-depleted GSCs (Figures S3E and S3F), supporting a non-overlapping role of IDs in GSCs. FACS analysis revealed that ID1 depletion in GSC8 and GSC2 reduced GSC markers NESTIN- and SOX2-positive cells, while increased cells expressing differentiation markers, such as S100β (an astrocyte marker), TUJ1 (neuronal cell marker), and O4 (oligodendrocyte marker) (Figures 5B and S4A), indicating ID1 as a differentiation inhibitor. To assess the tumorigenic role of ID1 in GSCs, we orthotopically implanted 1,000 control shRNA or ID1-KD GSCs into nude mice. After 40 days, neurological signs and brain tumors were observed in mice implanted with control shRNA GSC8 cells, but not in mice implanted with ID1-KD GSC8 cells (Figure 5C). We also assessed tumorigenic potential of ID1 by overexpressing ID1 in GSC5 cells that express endogenous ID1 similar to normal astrocyte cells (Figure S3A). The orthotopic injection of GSCs into nude mice showed that ID1-overexpressing GSC5 displayed faster tumor growth than control cells (Figure S5A).

We also confirmed that ID1 depletion in GSC8 cells increased the interactions of CULLIN3 with both DVL2 and GLI2, possibly due to increased CULLIN3 (Figure 5D). ID1 depletion in GSC8

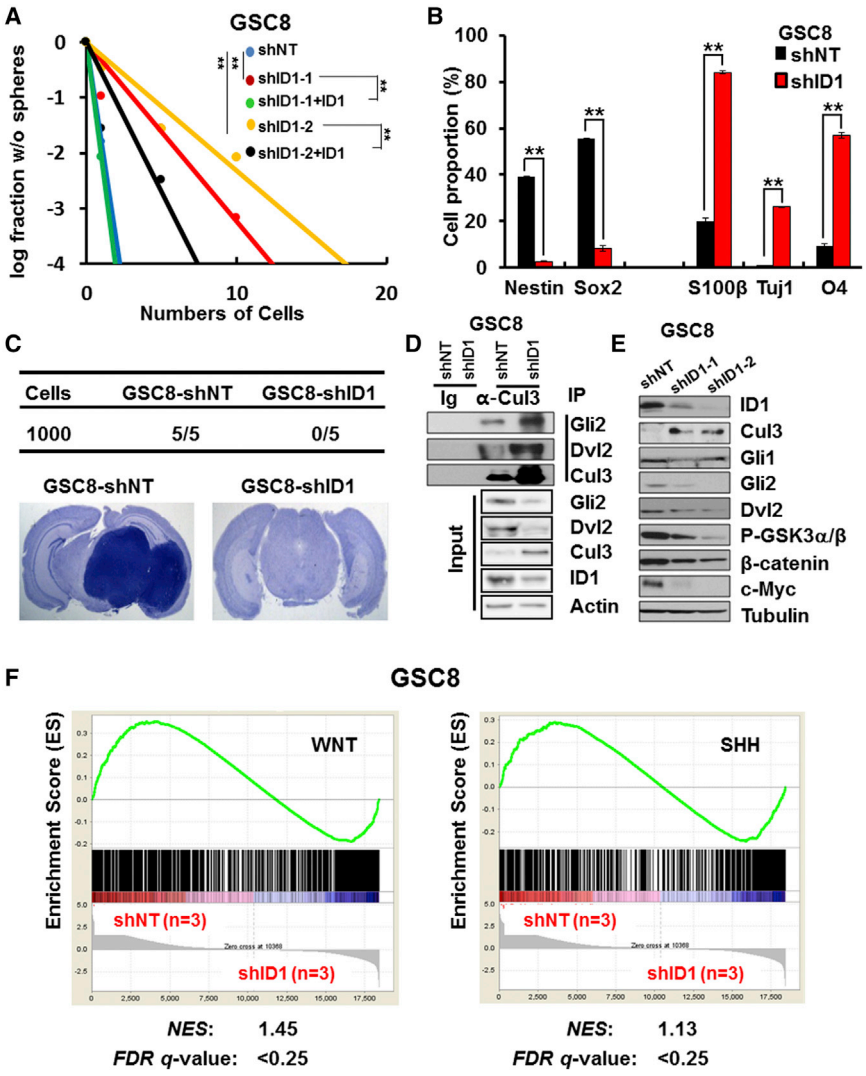

Figure 5. The Role of ID1 in the Maintenance of Human GSC Properties

(A) In vitro limiting dilution assays with different plating densities were used to determine the tumorsphere formation ability in GSC8 cells transduced with shNT, shID1-1 (3′ UTR targeted), and shID1-2 (3′ UTR targeted), and in ID1-CDS-overexpressing GSC8 cells transduced with shNT, shID1-1, and shID1-2. **$p < 0.01$ ($n = 24$).

(B) FACS showed cell proportions of NESTIN$^+$, SOX2$^+$, S100β$^+$, TUJ1$^+$, and O4$^+$ cells in ID1 knockdown and control GSC8. **$p < 0.01$ ($n = 3$). Data are mean ± SD.

(C) Tumor-forming frequency of ID1 knockdown and control GSCs 40 days post-orthotopic implantation (upper table). Representative H&E staining of mice whole brains implanted with ID1 knockdown and control GSCs (lower images).

(D) Interactions of endogenous CULLIN3 with GLI2 or DVL2 in GSC8 cells transduced with shNT and shID1.

(E) SHH and WNT signaling protein levels in GSC8 cells transduced with shNT, shID1-1, and shID1-2.

(F) Gene set enriched by WNT and SHH signaling was analyzed by GSEA in GSC8 transduced with shNT and shID1. NES, normalized enrichment score; FDR, false discovery rate *q* value.

and GSC2 cells reduced the downstream SHH and WNT signaling protein expression and ID1 overexpression in GSC5 cells increased the downstream SHH and WNT signaling protein expression (Figures 5E, S4B, and S5B). The qRT-PCR analysis revealed that ID1 did not significantly change *DVL2* and *GLI2* mRNA levels in GSC8 (Figure S5D), GSC2 (Figure S4C), and GSC5 cells (Figure S5C). Next, we conducted a gene set enrichment analysis (GSEA) of the downstream-response genes known to be regulated by SHH and WNT signaling pathways using microarray data of a control and ID1-KD GSCs. ID1 depletion in GSCs markedly repressed expression of genes enriched by SHH and WNT signaling pathways (Figures 5F and S4D). Taken together, these results indicate that ID1 is a key GSC regulator and activates SHH and WNT signaling pathways.

CULLIN3 Suppresses Cancer Stem Cell Properties and SHH/WNT Signaling in Primary Human GSCs

Next, we examined biological effects of CULLIN3 in GSC cells. CULLIN3 overexpression in GSC8 cells inhibited SHH and WNT signaling protein expression (Figure 6A). The luciferase reporter assays revealed that SHH and WNT/β-CATENIN signaling activities were decreased by CULLIN3 overexpression (Figure 6B). We also found that CULLIN3 overexpression led to marked decreases in expression of genes that are downstream of SHH (*GLI1*) and WNT (*c-MYC*) signaling pathways (Figure 6C). FACS analysis showed that CULLIN3 overexpression in GSC8 reduced stem cell marker-positive cells (NESTIN and SOX2), while increased cells expressing differentiation markers (S100β, TUJ1, and O4; Figure 6D). In vitro limiting dilution assay revealed that CULLIN3 overexpression significantly reduced tumorsphere-forming ability of GSC8 cells (Figure 6E). To elucidate the tumorigenic role of CULLIN3 in GSCs, we orthotopically implanted 1,000 control or CULLIN3-overexpressing GSCs into nude mice. After 40 days, neurological signs and brain tumors were observed in mice implanted with control GSC8 cells, but not in mice implanted with CULLIN3-overexpressing GSC8 cells (Figure 6F). Taken together, these results indicate that CULLIN3 is a key suppressor for GSCs and inhibits SHH and WNT signaling pathways.

Clinical Relevance of an ID1-CULLIN3 Expression Signature

To assess the clinical relevance of ID1 and CULLIN3, we first analyzed ID1 and CULLIN3 expression in various tumor types, WHO grades, GBM DNA methylation status, and GBM subtypes in the National Cancer Institute's Repository for Molecular Brain Neoplasia Data (REMBRANDT; Madhavan et al., 2009;

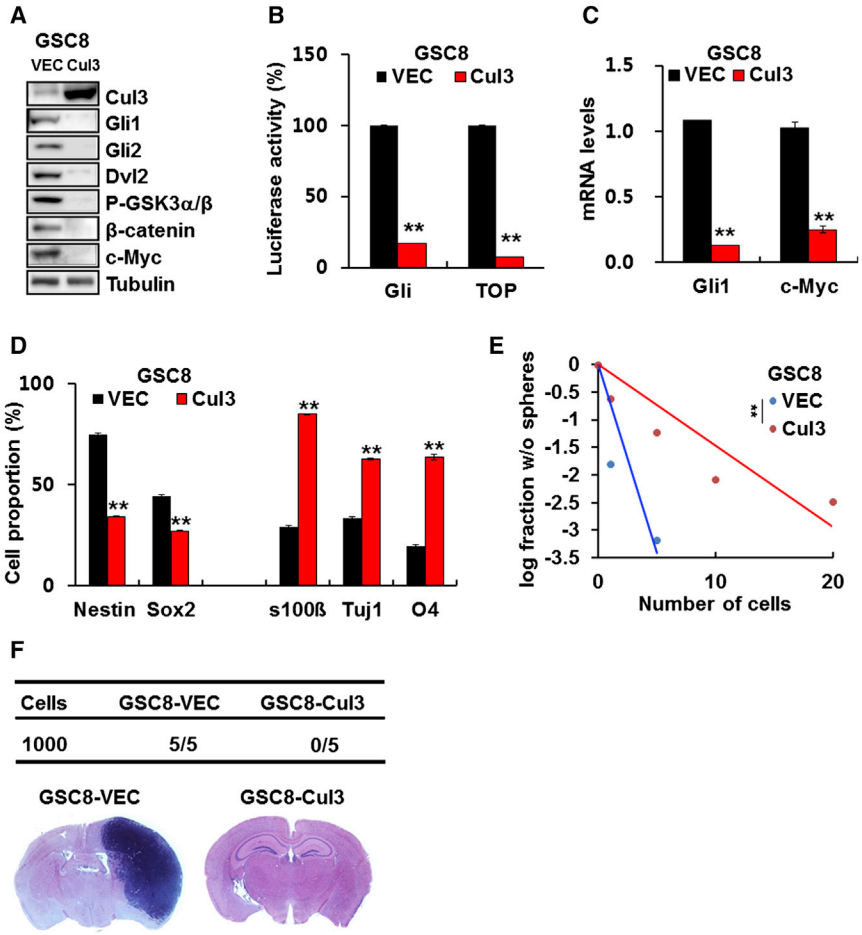

Figure 6. The Role of CULLIN3 in the Maintenance of Human GSC Properties

(A) SHH and WNT signaling protein levels in control GSC8 (VEC) and GSC8-CULLIN3 cells.

(B) Control GSC8 (VEC) and GSC8-CULLIN3 cells were transfected with pGL3-Gli-BS (containing Gli-binding sites) or pTOP-FLASH (containing TCF/LEF-binding sites) vectors. **$p < 0.01$ ($n = 3$). Data are mean ± SD.

(C) SHH and WNT signaling-downstream genes in control GSC8 and GSC8-CULLIN3 cells. Data are mean ± SD.

(D) FACS showed cell proportions of NESTIN$^+$, SOX2$^+$, S100β$^+$, TUJ1$^+$, and O4$^+$ cells in control GSC8 and GSC8-CULLIN3 cells. **$p < 0.01$ ($n = 3$). Data are mean ± SD.

(E) In vitro limiting dilution assays with different plating densities were used to determine the tumorsphere formation ability in control GSC8 and GSC8-CULLIN3 cells. **$p < 0.01$ ($n = 24$).

(F) Tumor-forming frequency of control GSC8 and GSC8-CULLIN3 cells 40 days post-orthotopic implantation (upper table). Representative H&E staining of mice whole brains implanted with control GSC8 and GSC8-CULLIN3 (lower images).

Figure S6A). As shown in Figure 7A, ID1 expression levels were significantly increased in all classifications of gliomas including astrocytoma, oligodendroglioma, WHO grade II and III gliomas, and grade IV GBMs compared to non-malignant brain tissues (Figures S6B and S6F), whereas CULLIN3 expression was significantly reduced in all gliomas (Figures S6C and S6G). Interestingly, ID1 and CULLIN3 expression remained significantly anticorrelated in the WHO grade IV GBM patient group, the relationship was not significant in lower-grade glioma groups such as astrocytoma, oligodendroglioma, and WHO grade II and III gliomas themselves, indicating that ID1-CULLIN3 signaling pathway might be more activated in GSC-enriched high-grade gliomas, GBMs (Figures 7B, S6D, and S6E). Furthermore, CULLIN3 high expression groups including ID1^{hi}/CUL3^{hi} and ID1^{lo}/CUL3^{hi} in all gliomas significantly extended patient survival compared to ID1^{hi}/CUL3^{lo} and ID1^{lo}/CUL3^{lo} groups (Figures S6H and S6I). In GBM, ID1 expression was significantly increased in classical subtype samples compared to neural subtype tumors (Figures 7A and S6J), but CULLIN3 expression was significantly decreased in classical and mesenchymal subtypes compared to proneural and neural subtypes (Figures 7A and S6K). ID1 and CULLIN3 expression exhibited a strong negative correlation in proneural subtype samples (Figures 7B and S6L). Furthermore, grouping patients according to ID1 and CULLIN3 expression in GBM displayed that the ID1^{lo}/Cul3^{hi} patient group comprising 44% neural, 30% proneural, 21% classical, and 5% mesenchymal GBM subtypes was significantly independent from ID1^{hi}/CUL3^{lo} and ID1^{lo}/CUL3^{lo} groups, which were composed of high percentage of classical and mesenchymal subtypes (Figure 7C). Indeed, the ID1^{hi}/CUL3^{lo} group exhibited a significantly poorer patient survival compared to the ID1^{lo}/CUL3^{hi} group (Figures 7D and S6M). To further evaluate the clinical significance of the ID1-CULLIN3 signature, we performed multivariate analyses considering age, radiotherapy, chemotherapy, surgery, and ID1/CULLIN3 expression levels in 186 glioblastoma specimens (full information for patients is provided in the REMBRANDT database). As shown in Table S1, ID1/CULLIN3 expression levels and age can be used as two independent prognostic markers for GBM patient survival. Thus, the prognostic significance of the ID1:CULLIN3 ratio supports the clinical relevance of this signaling axis.

To assess whether the ID1 and CULLIN3 expression correlates with SHH and WNT signaling activation in glioma patient samples, we analyzed the correlation between ID1 or CULLIN3 expression and HH or WNT signature (analyzed by single sample GSEA with SHH and WNT gene set in Figures 5F and S4D), ligands, and receptors (Figure 7E). SHH and WNT signatures showed significant positive and negative correlations with ID1 and CULLIN3 expression, respectively, but ligands and receptors did not exhibit correlation with ID1 and CULLIN3 expression, indicating that the ID1-CULLIN3 axis might regulate SHH and WNT signaling in ligand-independent manner. Conversely, desert hedgehog (DHH), WNT11, and WNT8A showed significant negative correlation with ID1 and CULLIN3 expression,

indicating that these HH and WNT ligands may contribute to poor overall survival of the ID1^{lo}/CUL3^{lo} glioma patient group (Figures S6H and S6I).

Pharmacological Blockade of Intracellular SHH/WNT Signaling and a Ligand-Independent Activation of SHH/WNT Signaling by ID1-CULLIN3 Axis

To directly evaluate whether the ID1-CULLIN3 axis acts as a ligand-independent SHH/WNT signaling regulator, we first inhibited WNT and SHH receptor signaling molecules, LRP5/6 and Smoothened, by treatment with siLRP5/6 (Figure S7A) and cyclopamine, respectively, in GSC5-VEC and GSC5-ID1 cells. Then, these cells were transfected with pTOP-FLASH-luciferase and Gli-BS-luciferase vectors. After treatment of WNT and SHH ligands (WNT3a and SHH-N), WNT and SHH signaling activities were examined by analyzing luciferase activity. The pTOP and Gli-BS luciferase activities in GSC5-VEC cells induced by WNT3a and SHH-N treatment were significantly decreased upon siLRP5/6 and cyclopamine treatment (Figures 7F and 7G). However, compared to GSC5-VEC cells, GSC5-ID1 cells treated with WNT3a and SHH-N or siLRP5/6 and cyclopamine did not exhibit any change in the markedly increased pTOP and Gli-BS luciferase activities (Figures 7F and 7G). These results indicate that ID1 regulates a ligand-independent activation of WNT and SHH signaling pathways. Next, we examined tumorsphere-forming ability of *Ink4a/Arf*$^{-/-}$ astrocyte-ID1 and GSC8 cells by treating them with JW67 (intracellular WNT signaling inhibitor), GANT61 (intracellular SHH signaling inhibitor), and combinatorial treatments (JW67+GANT61). Although single treatments of JW67 and GANT61 significantly reduced tumorsphere forming ability of *Ink4a/Arf*$^{-/-}$ astrocyte-ID1 and GSC8 cells compared to DMSO treatment, combinatorial treatment showed most significant suppression of tumorsphere forming ability (Figures 7H, 7I, S7B, and S7C). To assess biological roles of SHH and WNT signaling on GSCs' genesis, we overexpressed β-CATENIN S37A (a constitutively active form) and GLI2 in *Ink4a/Arf*$^{-/-}$ astrocyte-CYCLIN E cells that do not display GSCs' features (Figures 2 and S7D, inset). The β-CATENIN S37A and GLI2 markedly induced in vitro tumorsphere formation (Figure S7D) and in vivo subcutaneous tumor formation (Figure S7E). However, overexpression of β-CATENIN S37A and GLI2 in control *Ink4a/Arf*$^{-/-}$ astrocyte cells did not give rise to tumors at the same experimental conditions (data not shown). These results indicate that simultaneous induction of SHH and WNT signaling pathways by ID1-CULLIN3 regulatory axis plays a crucial role in maintaining GSC properties, suggesting that the combined inhibition of multiple stem cell signaling pathways should be an effective treatment strategy for GSC-enriched glioblastoma. Overall, our results suggest that ID1-mediated CULLIN3 suppression leads to a cell-autonomous acquisition of cancer stem cell signaling by direct activation of cell proliferation and ligand-independent WNT/SHH signaling through CYCLIN E, GLI2, and DVL2 protein stabilization.

DISCUSSION

Current molecularly targeted therapeutics against cancer stem cells exploits the core regulation of embryonic and tissue-specific stem cells. NOTCH, WNT, HEDGEHOG, and PI3K are some pathways that promote stem cell self-renewal. Inhibitors of these pathways often enter clinical trials with early promising results, even against glioblastoma; however, they eventually culminate in failure (Wen and Kesari, 2008; Takebe et al., 2011). Thus, paradigms focusing on signaling nodes, which control multiple elements of stem cell signaling, may be beneficial. In this study, we demonstrate that ID1 regulates SHH/WNT signaling through suppressing CULLIN3-mediated GLI2 and DVL2 protein degradation and suggest that ID1-CULLIN3 is an important signaling node in multiple core stem cell signaling pathways, converging on a single restriction point and demonstrating direct clinical implications.

Proteasome proteolysis is an intracellular autonomous mechanism to control essential cellular functions, including cell-cycle regulation and signal transduction. Inactivation of proteasome proteolysis stabilizes several proto-oncogenic and stem cell factors, including many IDs (Williams et al., 2011), TGF-β receptor I (Eichhorn et al., 2012), and REST (Huang et al., 2011). Furthermore, although GLI1 and DVL2 expression levels are both upregulated in malignant gliomas (Clement et al., 2007; Pulvirenti et al., 2011), activation of SHH/WNT signaling components by genetic mutations have not yet been reported. Our studies demonstrated that CULLIN3 interacts with and degrades SHH/WNT intracellular signaling transmitters, such as GLI2 and DVL2, by poly-unbiquitination-mediated proteolysis, indicating that the ID1-CULLIN3 axis activates SHH/WNT signaling pathways in an environmentally independent manner. In this signaling cascade, ID1 and CULLIN3 are the master switches for multi-intracellular signaling pathways.

Our findings show that GSCs could be generated and maintained by simultaneous control of multiple ligand/receptor-independent, intracellular stem cell signaling networks activated by deregulated proteolysis. Thus, directional manipulation of multi-signaling network nodes, such as the ID1-CULLIN3 signaling axis, should be applicable to the development of a treatment strategy that targets GSCs for the effective eradication of glioblastoma.

EXPERIMENTAL PROCEDURES

Cell Cultures

Normal human astrocytes (NHAs; Cambrex Bio Science) were maintained in astrocyte growth medium from an AGM-Astrocyte Medium Bullet Kit (Cambrex Bio Science). Murine *Ink4a/Arf*$^{-/-}$ astrocytes were isolated from the cerebral cortices of 5-day-old *Ink4a/Arf*$^{-/-}$ knockout mice and were maintained in DMEM enriched with 10% fetal bovine serum (FBS; HyClone). GSC1(X01), GSC2(X02), and GSC3(X03) were obtained from Dr. A. Soeda (Soeda et al., 2009); GSC4 (436), GSC5 (448), GSC6 (559T), and GSC8 were obtained from Dr. D. Nam (Joo et al., 2008); GSC7 (Aju14) was obtained from Dr. S. Kim (Jeon et al., 2014); and IN83 and IN1123 were obtained from Dr. I. Nakano (Jijiwa et al., 2011). All tested GSCs were cultured using neurobasal medium (Invitrogen) supplemented with modified N2, B27, epidermal growth factor (EGF, 20 ng/ml; R&D Systems), and basic fibroblast growth factor (bFGF, 20 ng/ml; R&D Systems). Cell growth and tumorsphere formation assays were performed as described previously (Jeon et al., 2008). The tumorsphere forming ability of in vitro limiting dilution assays was evaluated using the extreme limiting dilution analysis function (http://bioinf.wehi.edu.au/software/elda/). Cells were treated with GANT61 (Gli antagonist; 5.5 and 10 μM; Tocris Bioscience; Lauth et al., 2007) and JW67 (β-catenin inhibitor; 4.1 and 16.1 μM;

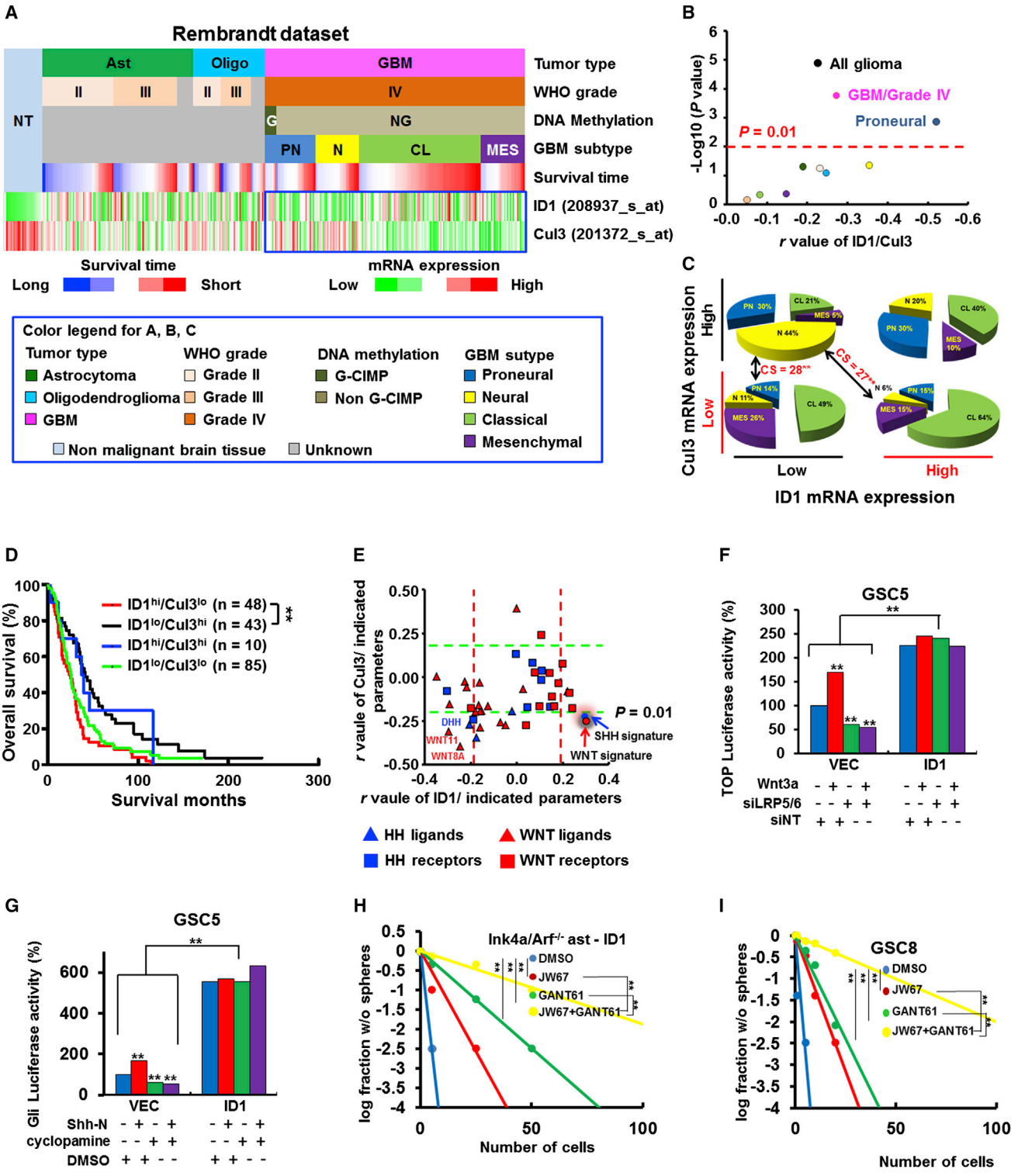

Figure 7. The ID1-CULLIN3 Expression Profile Acts as a Prognostic Indicator for Brain Tumor Patients

(A) Heatmap showing ID1, CULLIN3 expression, and patient survival time in tumor types, WHO grades, GBM DNA methylation status, GBM subtypes in REMBRANDT database.

(B) Dot plot showing correlation coefficients (*r* values) of ID1 and CULLIN3 expression in tumor types, WHO grades, GBM DNA methylation status, GBM subtypes in REMBRANDT database.

(legend continued on next page)

Tocris Bioscience; Waaler et al., 2011) for 2 weeks to monitor limiting dilution assays. Cells were treated with siNT (50 nM; Sigma; SIC001), siLRP5/6 (used for WNT receptor inactivation; 50 nM; Sigma; Hs01-00086820/Hs01-00039493), cyclopamine (Smoothened inhibitor; 10 μM; Sigma), human sonic hedgehog (Shh-N; 1 μg/ml; R&D Systems), and human WNT3a (100 ng/ml; R&D Systems).

Immunoblot Assays

Protein (30–100 μg) was resolved by 10% SDS-PAGE (NuPAGE Bis-Tris gel, Invitrogen) and transferred to polyvinylidene fluoride (PVDF) membranes (Millipore). The membranes were blocked with 5% non-fat milk and incubated with specific antibodies against target proteins (antibodies used are listed in Table S4). Cells were treated with cycloheximide (CHX, 50 μM; Cell Signaling Technology) to detect CYCLIN E, DVL2, and GLI2 protein stability.

Orthotopic Implantation Assay

Cells (10^2 and 10^4) were stereotactically injected into the left striata of nude mice (BALB/c nu/nu mice) for orthotopic implantation (coordinates: anterior-posterior, +2; medial-lateral, +2; dorsal-ventral, –3 mm from the bregma). All mouse experiments were approved by the animal care committee of Korea University and were performed in accordance with government and institutional guidelines and regulations.

Microarray and Gene Set Enrichment Analysis

Gene expression profiling was performed using HumanRef-8 v3 Expression BeadChips (Illumina) with 24,526 transcript probes. The samples were prepared according to the manufacturer's recommendations (Illumina). Array data export processing and analysis was performed using Illumina GenomeStudio v.20092 (Gene Expression Module v.1.5.4). GSEA (https://www.broadinstitute.org/gsea/) was used to analyze the enrichment of signaling target genes that are upregulated by WNT and SHH.

REMBRANDT Data Analysis

The Repository of Molecular Brain Neoplasia Data (REMBRANDT) (Madhavan et al., 2009) database was used to analyze correlations between clinical characteristics, survival, and gene expression in glioma specimens. The study flow is described in Figure S6. Patient groups were divided according to above and below the mean of ID1 (probe 208937_s_at)/Cullin3 (probe 201372_s_at) expression levels.

Statistical Analysis

Student's t tests were used to analyze statistical significance in the paired groups. One-way ANOVA was used to analyze statistical significance in multiple groups (more than two groups). Overall survival of glioblastoma patients was reported using Kaplan-Meier curves and significance was determined by log-rank analysis. Cox proportional hazard modeling was used to perform univariate and multivariate analyses. Data are expressed as means and 95% confidence intervals (CIs). All statistical tests were two sided, and $p < 0.05$ was statistically significant.

Soft-Agar Assay, Plasmids and Gene Transduction, RT-PCR, Immunofluorescence Assay and H&E Staining, FACS Analysis, Subcutaneous Implantation Assay, Immunoprecipitation, Denature Immunoprecipitation, and MALDI-TOF Assay

Detailed experimental procedures are provided in the Supplemental Information.

ACCESSION NUMBERS

The accession number for microarray data reported in this paper is GEO: GSE40614.

SUPPLEMENTAL INFORMATION

Supplemental Information includes Supplemental Experimental Procedures, seven figures, and four tables and can be found with this article online at http://dx.doi.org/10.1016/j.celrep.2016.06.092.

AUTHOR CONTRIBUTIONS

X.J. and H.K. designed experiments; X.J., H.-M.J., and H.K. wrote the manuscript; X.J., H.-M.J., and X.J. performed most experiments and analyzed data; J.Y., H.-Y.J., Y.-W.S., and S.-Y.O. helped in mouse works; J.-K.K., E.-J.K., S.-H.K., J.-E.J., and S.K. were involved with in vitro cell experiments; K.-F.T. and Y.X. provided key experimental materials; J.R. provided key experimental advice; and H.K. directed this study.

ACKNOWLEDGMENTS

This work was supported by grants from the National Research Foundation of Korea (NRF), funded by the Ministry of Education, Science, and Technology of Korea (2011-0017544), the Korea Health Technology R&D Project through the Korea Health Industry Development Institute (KHIDI), funded by the Ministry of Health & Welfare, Republic of Korea (HI12C1718), and Korea University. J.N.R. is supported by National Institute of Health grants CA154130, CA169117, CA171632, NS087913, and NS089272 and the James S. McDonnel foundation. X.J. was supported by a grant from the General Program of the National Natural Science Foundation of China (no. 81572891). We thank Ji-Hyun Kim (Soonchunhyang University) for providing graphic abstract. We thank Dr. A Soeda for providing GSC1(X01), GSC2(X02), and GSC3(X03) cells.

Received: November 8, 2015
Revised: March 25, 2016
Accepted: June 27, 2016
Published: July 28, 2016

REFERENCES

Anido, J., Sáez-Borderías, A., Gonzàlez-Juncà, A., Rodón, L., Folch, G., Carmona, M.A., Prieto-Sánchez, R.M., Barba, I., Martínez-Sáez, E., Prudkin,

(C) Pie graph showing GBM subtype composition in patient groups divided according to ID1 and Cul3 expression in REMBRANDT database. CS, Chi-square value, **$p < 0.01$.
(D) Kaplan-Meier survival curves of patient groups divided according to ID1 and CULLIN3 expression in REMBRANDT GBM dataset. Superscript "hi" and "lo" indicated high and low expression. Log rank **$p < 0.01$.
(E) Rank-ordered list of correlation coefficients (*r* values) between HH or WNT signature, ligands, receptors and ID1, or CULLIN3 expressions in REMBRANDT database.
(F) GSC5-VEC and GSC5-ID1 cells were treated with siNT or siLRP5/6 for 1 day and then transfected with pTOP-FLASH-luciferase vector. After treatment of WNT3a for 1 day, WNT signaling activity in these cells was examined by analyzing luciferase activity. **$p < 0.01$ ($n = 3$). Data are mean ± SD.
(G) GSC5-VEC and GSC5-ID1 cells were treated with DMSO or cyclopamine for 1 day and then transfected with pGL3-Gli-BS-luciferase vector. After treatment of SHH-N for 1 day, SHH signaling activity in these cells was examined by analyzing luciferase activity. **$p < 0.01$ ($n = 3$). Data are mean ± SD.
(H and I) In vitro limiting dilution assays with different plating densities were used to determine the tumorsphere formation ability in *Ink4a/Arf*$^{-/-}$ astrocytes-ID1 (H) and GSC8 cells (I) treated with JW67 (*Ink4a/Arf*$^{-/-}$ astrocytes-ID1; 4.1 μM, GSC8; 16.1 μM), GANT61 (*Ink4a/Arf*$^{-/-}$ astrocytes-ID1; 10 μM, GSC8; 5.5 μM), and combinatorial treatments (JW67+GANT61). **$p < 0.01$ ($n = 24$).

L., et al. (2010). TGF-β receptor inhibitors target the CD44(high)/Id1(high) glioma-initiating cell population in human glioblastoma. Cancer Cell *18*, 655–668.

Becher, O.J., Hambardzumyan, D., Fomchenko, E.I., Momota, H., Mainwaring, L., Bleau, A.M., Katz, A.M., Edgar, M., Kenney, A.M., Cordon-Cardo, C., et al. (2008). Gli activity correlates with tumor grade in platelet-derived growth factor-induced gliomas. Cancer Res. *68*, 2241–2249.

Bleau, A.M., Hambardzumyan, D., Ozawa, T., Fomchenko, E.I., Huse, J.T., Brennan, C.W., and Holland, E.C. (2009). PTEN/PI3K/Akt pathway regulates the side population phenotype and ABCG2 activity in glioma tumor stem-like cells. Cell Stem Cell *4*, 226–235.

Cancer Genome Atlas Research Network (2008). Comprehensive genomic characterization defines human glioblastoma genes and core pathways. Nature *455*, 1061–1068.

Clement, V., Sanchez, P., de Tribolet, N., Radovanovic, I., and Ruiz i Altaba, A. (2007). HEDGEHOG-GLI1 signaling regulates human glioma growth, cancer stem cell self-renewal, and tumorigenicity. Curr. Biol. *17*, 165–172.

Dell'albani, P., Rodolico, M., Pellitteri, R., Tricarichi, E., Torrisi, S.A., D'Antoni, S., Zappia, M., Albanese, V., Caltabiano, R., Platania, N., et al. (2014). Differential patterns of NOTCH1-4 receptor expression are markers of glioma cell differentiation. Neuro-oncol. *16*, 204–216.

Eichhorn, P.J., Rodón, L., Gonzàlez-Juncà, A., Dirac, A., Gili, M., Martínez-Sáez, E., Aura, C., Barba, I., Peg, V., Prat, A., et al. (2012). USP15 stabilizes TGF-β receptor I and promotes oncogenesis through the activation of TGF-β signaling in glioblastoma. Nat. Med. *18*, 429–435.

Eyler, C.E., Wu, Q., Yan, K., MacSwords, J.M., Chandler-Militello, D., Misuraca, K.L., Lathia, J.D., Forrester, M.T., Lee, J., Stamler, J.S., et al. (2011). Glioma stem cell proliferation and tumor growth are promoted by nitric oxide synthase-2. Cell *146*, 53–66.

Guryanova, O.A., Wu, Q., Cheng, L., Lathia, J.D., Huang, Z., Yang, J., MacSwords, J., Eyler, C.E., McLendon, R.E., Heddleston, J.M., et al. (2011). Nonreceptor tyrosine kinase BMX maintains self-renewal and tumorigenic potential of glioblastoma stem cells by activating STAT3. Cancer Cell *19*, 498–511.

Huang, Z., Wu, Q., Guryanova, O.A., Cheng, L., Shou, W., Rich, J.N., and Bao, S. (2011). Deubiquitylase HAUSP stabilizes REST and promotes maintenance of neural progenitor cells. Nat. Cell Biol. *13*, 142–152.

Jeon, H.M., Jin, X., Lee, J.S., Oh, S.Y., Sohn, Y.W., Park, H.J., Joo, K.M., Park, W.Y., Nam, D.H., DePinho, R.A., et al. (2008). Inhibitor of differentiation 4 drives brain tumor-initiating cell genesis through cyclin E and notch signaling. Genes Dev. *22*, 2028–2033.

Jeon, H.M., Kim, S.H., Jin, X., Park, J.B., Kim, S.H., Joshi, K., Nakano, I., and Kim, H. (2014). Crosstalk between glioma-initiating cells and endothelial cells drives tumor progression. Cancer Res. *74*, 4482–4492.

Jijiwa, M., Demir, H., Gupta, S., Leung, C., Joshi, K., Orozco, N., Huang, T., Yildiz, V.O., Shibahara, I., de Jesus, J.A., et al. (2011). CD44v6 regulates growth of brain tumor stem cells partially through the AKT-mediated pathway. PLoS ONE *6*, e24217.

Jin, X., Yin, J., Kim, S.H., Sohn, Y.W., Beck, S., Lim, Y.C., Nam, D.H., Choi, Y.J., and Kim, H. (2011). EGFR-AKT-Smad signaling promotes formation of glioma stem-like cells and tumor angiogenesis by ID3-driven cytokine induction. Cancer Res. *71*, 7125–7134.

Jin, X., Kim, S.H., Jeon, H.M., Beck, S., Sohn, Y.W., Yin, J., Kim, J.K., Lim, Y.C., Lee, J.H., Kim, S.H., et al. (2012). Interferon regulatory factor 7 regulates glioma stem cells via interleukin-6 and Notch signalling. Brain *135*, 1055–1069.

Joo, K.M., Kim, S.Y., Jin, X., Song, S.Y., Kong, D.S., Lee, J.I., Jeon, J.W., Kim, M.H., Kang, B.G., Jung, Y., et al. (2008). Clinical and biological implications of CD133-positive and CD133-negative cells in glioblastomas. Lab. Invest. *88*, 808–815.

Kim, S.H., Kim, E.J., Hitomi, M., Oh, S.Y., Jin, X., Jeon, H.M., Beck, S., Jin, X., Kim, J.K., Park, C.G., et al. (2015). The LIM-only transcription factor LMO2 determines tumorigenic and angiogenic traits in glioma stem cells. Cell Death Differ. *22*, 1517–1525.

Lathia, J.D., Mack, S.C., Mulkearns-Hubert, E.E., Valentim, C.L., and Rich, J.N. (2015). Cancer stem cells in glioblastoma. Genes Dev. *29*, 1203–1217.

Lauth, M., Bergström, A., Shimokawa, T., and Toftgård, R. (2007). Inhibition of GLI-mediated transcription and tumor cell growth by small-molecule antagonists. Proc. Natl. Acad. Sci. USA *104*, 8455–8460.

Lyden, D., Young, A.Z., Zagzag, D., Yan, W., Gerald, W., O'Reilly, R., Bader, B.L., Hynes, R.O., Zhuang, Y., Manova, K., and Benezra, R. (1999). Id1 and Id3 are required for neurogenesis, angiogenesis and vascularization of tumour xenografts. Nature *401*, 670–677.

Madhavan, S., Zenklusen, J.C., Kotliarov, Y., Sahni, H., Fine, H.A., and Buetow, K. (2009). Rembrandt: helping personalized medicine become a reality through integrative translational research. Mol. Cancer Res. *7*, 157–167.

Munoz, J.L., Rodriguez-Cruz, V., Ramkissoon, S.H., Ligon, K.L., Greco, S.J., and Rameshwar, P. (2015). Temozolomide resistance in glioblastoma occurs by miRNA-9-targeted PTCH1, independent of sonic hedgehog level. Oncotarget *6*, 1190–1201.

Niola, F., Zhao, X., Singh, D., Castano, A., Sullivan, R., Lauria, M., Nam, H.S., Zhuang, Y., Benezra, R., Di Bernardo, D., et al. (2012). Id proteins synchronize stemness and anchorage to the niche of neural stem cells. Nat. Cell Biol. *14*, 477–487.

Niola, F., Zhao, X., Singh, D., Sullivan, R., Castano, A., Verrico, A., Zoppoli, P., Friedmann-Morvinski, D., Sulman, E., Barrett, L., et al. (2013). Mesenchymal high-grade glioma is maintained by the ID-RAP1 axis. J. Clin. Invest. *123*, 405–417.

Pulvirenti, T., Van Der Heijden, M., Droms, L.A., Huse, J.T., Tabar, V., and Hall, A. (2011). Dishevelled 2 signaling promotes self-renewal and tumorigenicity in human gliomas. Cancer Res. *71*, 7280–7290.

Qiang, L., Wu, T., Zhang, H.W., Lu, N., Hu, R., Wang, Y.J., Zhao, L., Chen, F.H., Wang, X.T., You, Q.D., and Guo, Q.L. (2012). HIF-1α is critical for hypoxia-mediated maintenance of glioblastoma stem cells by activating Notch signaling pathway. Cell Death Differ. *19*, 284–294.

Rheinbay, E., Suvà, M.L., Gillespie, S.M., Wakimoto, H., Patel, A.P., Shahid, M., Oksuz, O., Rabkin, S.D., Martuza, R.L., Rivera, M.N., et al. (2013). An aberrant transcription factor network essential for Wnt signaling and stem cell maintenance in glioblastoma. Cell Rep. *3*, 1567–1579.

Ruiz i Altaba, A. (1998). Combinatorial Gli gene function in floor plate and neuronal inductions by Sonic hedgehog. Development *125*, 2203–2212.

Singer, J.D., Gurian-West, M., Clurman, B., and Roberts, J.M. (1999). Cullin-3 targets cyclin E for ubiquitination and controls S phase in mammalian cells. Genes Dev. *13*, 2375–2387.

Singh, S.K., Hawkins, C., Clarke, I.D., Squire, J.A., Bayani, J., Hide, T., Henkelman, R.M., Cusimano, M.D., and Dirks, P.B. (2004). Identification of human brain tumour initiating cells. Nature *432*, 396–401.

Soeda, A., Park, M., Lee, D., Mintz, A., Androutsellis-Theotokis, A., McKay, R.D., Engh, J., Iwama, T., Kunisada, T., Kassam, A.B., et al. (2009). Hypoxia promotes expansion of the CD133-positive glioma stem cells through activation of HIF-1alpha. Oncogene *28*, 3949–3959.

Takebe, N., Harris, P.J., Warren, R.Q., and Ivy, S.P. (2011). Targeting cancer stem cells by inhibiting Wnt, Notch, and Hedgehog pathways. Nat. Rev. Clin. Oncol. *8*, 97–106.

Tanaka, S., Louis, D.N., Curry, W.T., Batchelor, T.T., and Dietrich, J. (2013). Diagnostic and therapeutic avenues for glioblastoma: no longer a dead end? Nat. Rev. Clin. Oncol. *10*, 14–26.

Waaler, J., Machon, O., von Kries, J.P., Wilson, S.R., Lundenes, E., Wedlich, D., Gradl, D., Paulsen, J.E., Machonova, O., Dembinski, J.L., et al. (2011). Novel synthetic antagonists of canonical Wnt signaling inhibit colorectal cancer cell growth. Cancer Res. *71*, 197–205.

Wen, P.Y., and Kesari, S. (2008). Malignant gliomas in adults. N. Engl. J. Med. *359*, 492–507.

Williams, S.A., Maecker, H.L., French, D.M., Liu, J., Gregg, A., Silverstein, L.B., Cao, T.C., Carano, R.A., and Dixit, V.M. (2011). USP1 deubiquitinates ID proteins to preserve a mesenchymal stem cell program in osteosarcoma. Cell *146*, 918–930.

Yan, K., Wu, Q., Yan, D.H., Lee, C.H., Rahim, N., Tritschler, I., DeVecchio, J., Kalady, M.F., Hjelmeland, A.B., and Rich, J.N. (2014). Glioma cancer stem cells secrete Gremlin1 to promote their maintenance within the tumor hierarchy. Genes Dev. *28*, 1085–1100.

Yang, W., Xia, Y., Ji, H., Zheng, Y., Liang, J., Huang, W., Gao, X., Aldape, K., and Lu, Z. (2011). Nuclear PKM2 regulates β-catenin transactivation upon EGFR activation. Nature *480*, 118–122.

Yi, L., Xiao, H., Xu, M., Ye, X., Hu, J., Li, F., Li, M., Luo, C., Yu, S., Bian, X., and Feng, H. (2011). Glioma-initiating cells: a predominant role in microglia/macrophages tropism to glioma. J. Neuroimmunol. *232*, 75–82.

Yin, J., Park, G., Kim, T.H., Hong, J.H., Kim, Y.J., Jin, X., Kang, S., Jung, J.E., Kim, J.Y., Yun, H., et al. (2015). Pigment epithelium-derived factor (PEDF) expression induced by EGFRvIII promotes self-renewal and tumor progression of glioma stem cells. PLoS Biol. *13*, e1002152.